

On the Modeling and Design of Dual-Stator Windings to Minimize Circulating Harmonic Currents for VSI Fed AC Machines

Djafar Hadiouche, Hubert Razik, *Senior Member, IEEE*, and Abderrezak Rezzoug, *Member, IEEE*

Abstract—The major drawback of usual dual-stator ac machines, when supplied by a voltage-source inverter (VSI), is the occurrence of extra harmonic currents. These extra currents circulate only in the stator windings and cause additional losses. This paper deals with the modeling and design of dual-stator winding ac machines for safe operation with a VSI. A new reference frame model for a dual-stator induction machine (DSIM), including mutual leakage coupling, is proposed. This model allows us to highlight the previously mentioned circulating harmonic currents. The leakage inductance associated with these harmonics is shown to have quite a small value, highly depending on the coil pitch. It is also shown that full pitch is required, and that special slot shape designs should be investigated, to limit the magnitude of circulating currents. Experimental results on a prototype of a DSIM are presented and they show a very good correlation with theoretical curves.

Index Terms—Dual-stator ac machines, experimentation, induction machine, modeling, multiwinding multiconverter systems, simulation, voltage-source inverter (VSI).

I. INTRODUCTION

SINCE the late 1920s [1], dual-stator ac machines have been used in many applications, for their advantages in power segmentation, reliability, and minimized torque pulsations. Such segmented structures are very attractive for high-power applications, since they allow the use of lower rating power electronic devices at a switching frequency higher than the one usually used in three-phase ac machine drives. Nevertheless, when dual-stator machines are driven by a voltage-source inverter (VSI), surprisingly large stator harmonic currents occur [6], [7], adding extra losses and require larger semiconductor device ratings. These large harmonic currents are caused by the small impedance for these harmonics [4], [8]–[10]. Clearly,

Paper IPCSD 03-119, presented at the 2001 Industry Applications Society Annual Meeting, Chicago, IL, September 30–October 5, and approved for publication in the IEEE TRANSACTIONS ON INDUSTRY APPLICATIONS by the Electric Machines Committee of the IEEE Industry Applications Society. Manuscript submitted for review October 15, 2001 and released for publication November 17, 2003.

D. Hadiouche was with the Groupe de Recherche en Electrotechnique et Electronique de Nancy, GREEN CNRS UMR 7037, Université Henri Poincaré, F-54506 Vandœuvre-lès-Nancy, Cedex, France. He is now with GE Fanuc Automation Europe S.A., L-6468 Echternach, Luxembourg (e-mail: djafar.hadiouche@wanadoo.fr).

H. Razik and A. Rezzoug are with the Groupe de Recherche en Electrotechnique et Electronique de Nancy, GREEN CNRS UMR 7037, Université Henri Poincaré, F-54506 Vandœuvre-lès-Nancy, Cedex, France (e-mail: Hubert.Razik@green.uhp-nancy.fr; Abderrezak.Rezzoug@green.uhp-nancy.fr).

Digital Object Identifier 10.1109/TIA.2004.824511

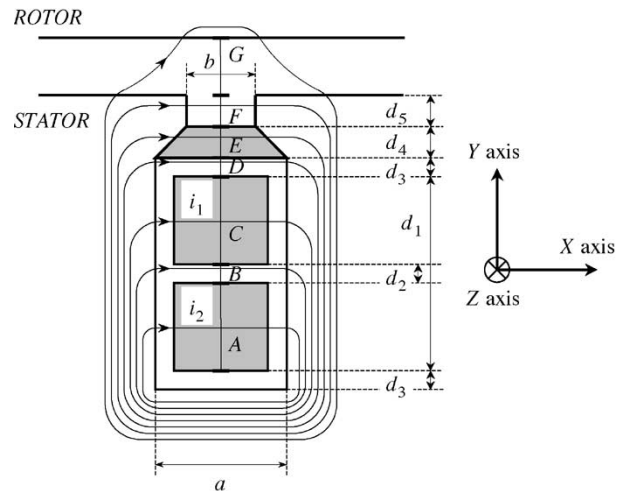


Fig. 1. Slot shape and leakage flux paths.

this drawback is in contradiction with the concept of power segmentation.

Therefore, it is of interest to study the machine inductances in detail, and how they vary with the stator winding design. It is the aim of this paper, where a new reference frame model for a dual-stator induction machine (DSIM), including mutual leakage coupling, is presented.

Experimental results on a prototype of DSIM are presented and they show a very good correlation with theoretical curves.

II. PRELIMINARY STUDY: SLOT LEAKAGE INDUCTANCES

Nowadays, the most commonly used methods to calculate machine inductances are finite-elements-based ones. However, it is always useful to make some analytical calculations because of their help in understanding the phenomenons [2], [3]. The slot shape used here for illustration is presented in Fig. 1. It is simple and may not be realistic for some of the current optimized machines, but it is sufficient to explain the existence of a mutual leakage coupling between different stator phases. It is not the aim of this paper to carry out calculations with complicated slot shapes, because the result would be quite the same.

Basically, the slot leakage flux for one coil is the flux through the total slot area, being the sum of areas A, B, C, D, E, F, and G (see traces in Fig. 1). Let us consider a closed path of integration crossing an area S. The path encloses $n_{S1}(Y)$ conductors of the top half of the slot and $n_{S2}(Y)$ conductors of the bottom

half. These conductors carry respectively the currents of phase 1 and phase 2. Starting from Ampere's Law with the assumption of linearity and infinite iron permeability, one can write

$$\int_{X_S(Y)} h_S(Y) dX = h_S(Y) X_S(Y) = n_{S1}(Y) i_1 + n_{S2}(Y) i_2 \quad (1)$$

where $h_S(Y)$ is the magnetic field along the path, created by the $n_{S1}(Y)$ and the $n_{S2}(Y)$ conductors. It is supposed to be only in the X -axis direction and unvarying with X (this is false for area G which is not considered in this study for simplicity).

The differential flux is

$$d\phi_S = \mu_0 h_S(Y) dS = \mu_0 h_S(Y) L dY \quad (2)$$

where L is the stack length, and μ_0 is the free space permeability. The differential flux for conductors of phase i is

$$d\phi_{Si} = n_{Si}(Y) d\phi_S. \quad (3)$$

Hence, the total flux through the area S , for the $n_{Si}(Y)$ conductors of phase i , is

$$\phi_{Si} = \mu_0 L \int_{Y_S} n_{Si}(Y) X_S^{-1}(Y) [n_{S1}(Y) i_1 + n_{S2}(Y) i_2] dY. \quad (4)$$

As an example, let us consider area C

$$\begin{aligned} X_C(Y) &= a, \\ Y_C &= \frac{(d_1 - d_2)}{2} \\ n_{C1}(Y) &= \frac{nc}{2} \left[\frac{(d_1 - d_2)}{2} \right]^{-1} Y \\ n_{C2}(Y) &= \frac{nc}{2}. \end{aligned}$$

Equation (4) results in

$$\begin{aligned} \phi_{C1} &= \frac{\mu_0 L}{a} \frac{(d_1 - d_2)}{2} \left(\frac{nc}{2} \right)^2 \left(\frac{i_1}{3} + \frac{i_2}{2} \right) \\ \phi_{C2} &= \frac{\mu_0 L}{a} \frac{(d_1 - d_2)}{2} \left(\frac{nc}{2} \right)^2 \left(\frac{i_1}{2} + i_2 \right) \end{aligned}$$

$(nc/2)$ being the total number of conductors of each half of the slot.

Following the same procedure for the other paths, the slot leakage flux for conductors of phase i is finally

$$\phi'_{li} = \sum_S \phi_{Si} = \phi_{Ai} + \phi_{Bi} + \phi_{Ci} + \phi_{Di} + \phi_{Ei} + \phi_{Fi}. \quad (5)$$

For one coil of phase 1, for example, it is shown that it can be put in the following form:

$$\phi'_{l1} = \left(\frac{nc}{2} \right)^2 P_t i_1 + \left(\frac{nc}{2} \right)^2 P_{tb} i_2 \quad (6)$$

where P_t and P_{tb} are the total slot permeances associated respectively with the top conductors and with the mutual coupling between top and bottom conductors.

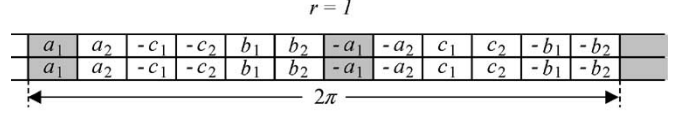


Fig. 2. Distribution of conductors for full-pitch dual-stator winding.

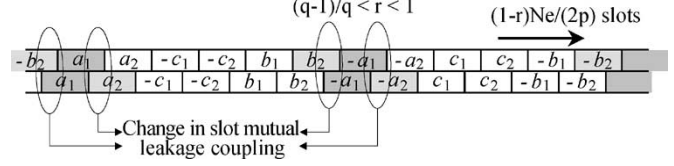


Fig. 3. Distribution of conductors for dual-stator winding with coil pitch $(q-1)/q < r < 1$.

Let us consider now the slot carrying the return conductors. Current i_1 is now flowing in the bottom of the slot and another current (i_3 for example) in the top. Therefore, the slot leakage flux becomes (P_b being the permeance for bottom conductors)

$$\phi''_{l1} = \left(\frac{nc}{2} \right)^2 P_b i_1 + \left(\frac{nc}{2} \right)^2 P_{tb} i_3. \quad (7)$$

Finally, the slot leakage flux linking one coil of $(nc/2)$ turns of phase 1 is

$$\phi_{l1} = \phi'_{l1} + \phi''_{l1} = (l_t + l_b) i_1 + m_{tb} i_2 + m_{tb} i_3. \quad (8)$$

Equation (8) gives the definition of the different slot leakage inductances of one coil. l_t represents the part of the slot "self-leakage" inductance related to top conductors, l_b is the one related to bottom conductors, and m_{tb} is the slot "mutual leakage" inductance between top and bottom conductors.

III. MODEL IN $(a_1 - b_1 - c_1 - a_2 - b_2 - c_2)$ FRAMES

In usual dual-stator windings, two sets of three-phase windings, spatially shifted by an electrical angle of 30° , share a common magnetic structure. The phases of stator 1 are named a_1, b_1 , and c_1 , and those of stator 2 are named a_2, b_2 , and c_2 . Let Ne be the number of slots, q the number of phases and r the coil pitch. Therefore, the number of slots per phase is Ne/q , which corresponds, in a double-layer winding, to the number of coils per phase. For full pitch (see Fig. 2), (8) becomes

$$\phi_{lsa1(r=1)} = [(l_t + l_b) + 2m_{tb}] i_{sa1}. \quad (9)$$

Hence, the slot leakage flux per phase for full pitch is

$$\Psi_{lsa1(r=1)} = \left(\frac{Ne}{q} \right) \phi_{lsa1(r=1)} \quad (10)$$

$$\Psi_{lsa1(r=1)} = [(L_t + L_b) + 2M_{tb}] i_{sa1} \quad (11)$$

where $(L_t + L_b)$ is the slot self-leakage inductance per phase, and $2M_{tb}$ is the slot mutual leakage inductance between top and bottom conductors, for one whole phase winding, for full pitch.

When the windings are pitched, one layer is displaced from the other by a certain number of slots. This results in a change of the slot mutual leakage coupling. From the example of Fig. 3, where the coil pitch is so that $(q-1)/q < r < 1$, the top layer

TABLE I
FUNCTIONS k_i IN THE MUTUAL LEAKAGE INDUCTANCE MATRIX [SEE (17)]

j	$k1$	$k2$	$k3$
1	$1-2k$	0	k
2	0	$-k$	$(1/2-k)$
3	0	$-(1/2-k)$	0
4	0	k	0
5	0	$(1/2-k)$	$-k$
6	$-2k$	0	$-(1/2-k)$
$k = q[(q-(j-1))/q - r]/2$			

is displaced by $(1-r)Ne/(2p)$ slots, where p is the number of pole pairs. The slot leakage flux becomes

$$\Psi lsa_1(\frac{2}{3} < r < 1) = \Psi lsa_1(r=1) + (1-r) \times \left(\frac{Ne}{2p} \right) 2m_{tb}p(-2isa_1 + isa_2 - isb_2). \quad (12)$$

Starting from this analysis, one can derive the variation of the slot leakage flux for phase a_1 according to the coil pitch varying from 1 to 0. The fluxes for the remaining phases can be easily found by symmetry.

Finally, the slot leakage flux linked by the stator windings can be written in the following matrix form:

$$[\Psi ls] = \{[Lls] + [Mlss]\} [is] \quad (13)$$

where

$$[\Psi ls] = {}^t[\Psi lsa_1 \Psi lsb_1 \Psi lsc_1 \Psi lsa_2 \Psi lsb_2 \Psi lsc_2] \quad (14)$$

$$[is] = {}^t[isa_1 isb_1 isc_1 isa_2 isb_2 isc_2] \quad (15)$$

$$[Lls] = (L_t + L_b) \begin{bmatrix} 1 & 0 & 0 & 0 & 0 & 0 \\ 0 & 1 & 0 & 0 & 0 & 0 \\ 0 & 0 & 1 & 0 & 0 & 0 \\ 0 & 0 & 0 & 1 & 0 & 0 \\ 0 & 0 & 0 & 0 & 1 & 0 \\ 0 & 0 & 0 & 0 & 0 & 1 \end{bmatrix} \quad (16)$$

$$[Mlss] = 2M_{tb} \begin{bmatrix} k1 & k2 & k2 & k3 & -k3 & 0 \\ k2 & k1 & k2 & 0 & k3 & -k3 \\ k2 & k2 & k1 & -k3 & 0 & k3 \\ k3 & 0 & -k3 & k1 & k2 & k2 \\ -k3 & k3 & 0 & k2 & k1 & k2 \\ 0 & -k3 & k3 & k2 & k2 & k1 \end{bmatrix}. \quad (17)$$

k_i are functions of the coil pitch, being linear inside each of the six intervals defined by

$$\frac{(q-j)}{q} < r < \frac{(q-(j-1))}{q} \quad (18)$$

with $1 \leq j \leq q$. They are detailed in Table I.

IV. REFERENCE FRAME MODEL

A. Transformation Matrix

As for three-phase systems, the use of a transformation matrix [4]–[6] leads to express the variables in an orthogonal base. The transformation used here was already proposed in [5] for the study of DSIMs with an arbitrary shift angle α between the two sets of three-phase windings. It is given by (19), as shown at the bottom of the page, where, in this paper, α is set to $\pi/6$.

Using (19), the original six-dimensional stator system can be decomposed into three two-dimensional uncoupled subsystems. These are the usual $(d-q)$ one, a zero-sequence $(o_1 - o_2)$ one, and another nonelectromechanical energy-conversion-related one [4], [6], [8], [15]–[18], named $(x-y)$. The transformation has the property to separate harmonics into different groups and to project them into each subsystem. In the case studied here, where the two stator windings are spatially shifted by 30° , low-order harmonics such as the fifth and seventh are projected in the $(x-y)$ subsystem. This results in large stator circulating fifth and seventh harmonic currents [6], [7], especially when dual six-step VSI is used [6], [11], [12], because of the small impedance for these harmonics [4], [8]–[10]. These currents are at the origin of extra losses and require larger semiconductor device ratings. Therefore, the above-mentioned impedance should be as high as possible.

B. Model in $(d-q)(x-y)(o_1 - o_2)$ Frames

1) $(d-q)(x-y)(o_1 - o_2)$ Leakage Inductances: Applying the transformation matrix $[Ts(\alpha)]^{-1}$ to (13) results in the following transformed slot leakage uncoupled fluxes:

$${}^t[\Psi lsd \Psi lsq \Psi lxx \Psi lyy \Psi lso_1 \Psi lso_2] = [Ts(\alpha)]^{-1} \cdot {}^t[\Psi lsa_1 \Psi lsb_1 \Psi lsc_1 \Psi lsa_2 \Psi lsb_2 \Psi lsc_2] \quad (20)$$

and

$$\begin{aligned} \begin{bmatrix} \Psi lsd \\ \Psi lsq \end{bmatrix} &= (L_t + L_b) \begin{bmatrix} 1 + 2k_{mtb}(k1 - k2 + \sqrt{3}k3) \\ \times \begin{bmatrix} 1 & 0 \\ 0 & 1 \end{bmatrix} \begin{bmatrix} isd \\ isq \end{bmatrix} \end{bmatrix} \\ &= Llsdq \begin{bmatrix} 1 & 0 \\ 0 & 1 \end{bmatrix} \begin{bmatrix} isd \\ isq \end{bmatrix} \end{aligned} \quad (21)$$

$$\begin{aligned} \begin{bmatrix} \Psi lxx \\ \Psi lyy \end{bmatrix} &= (L_t + L_b) \begin{bmatrix} 1 + 2k_{mtb}(k1 - k2 - \sqrt{3}k3) \\ \times \begin{bmatrix} 1 & 0 \\ 0 & 1 \end{bmatrix} \begin{bmatrix} ixx \\ iyy \end{bmatrix} \end{bmatrix} \\ &= Llsxy \begin{bmatrix} 1 & 0 \\ 0 & 1 \end{bmatrix} \begin{bmatrix} ixx \\ iyy \end{bmatrix} \end{aligned} \quad (22)$$

$$[Ts(\alpha)]^{-1} = \frac{1}{\sqrt{3}} \begin{bmatrix} \cos(0) & \cos(\frac{2\pi}{3}) & \cos(\frac{4\pi}{3}) & \cos(\alpha) & \cos(\alpha + \frac{2\pi}{3}) & \cos(\alpha + \frac{4\pi}{3}) \\ \sin(0) & \sin(\frac{2\pi}{3}) & \sin(\frac{4\pi}{3}) & \sin(\alpha) & \sin(\alpha + \frac{2\pi}{3}) & \sin(\alpha + \frac{4\pi}{3}) \\ \cos(0) & \cos(\frac{4\pi}{3}) & \cos(\frac{2\pi}{3}) & \cos(\pi - \alpha) & \cos(\frac{\pi}{3} - \alpha) & \cos(\frac{5\pi}{3} - \alpha) \\ \sin(0) & \sin(\frac{4\pi}{3}) & \sin(\frac{2\pi}{3}) & \sin(\pi - \alpha) & \sin(\frac{\pi}{3} - \alpha) & \sin(\frac{5\pi}{3} - \alpha) \\ 1 & 1 & 1 & 0 & 0 & 0 \\ 0 & 0 & 0 & 1 & 1 & 1 \end{bmatrix} \quad (19)$$

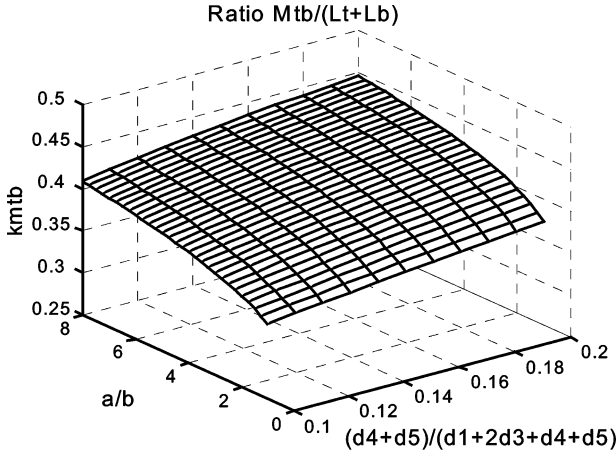


Fig. 4. Coefficient k_{mtb} versus slot dimensions (semiclosed slot of Fig. 1).

$$\begin{aligned} \begin{bmatrix} \Psi_{lso1} \\ \Psi_{lso2} \end{bmatrix} &= (L_t + L_b) [1 + 2k_{mtb}(k_1 + 2k_2)] \\ &\times \begin{bmatrix} 1 & 0 \\ 0 & 1 \end{bmatrix} \begin{bmatrix} iso_1 \\ iso_2 \end{bmatrix} \\ &= L_{lso} \begin{bmatrix} 1 & 0 \\ 0 & 1 \end{bmatrix} \begin{bmatrix} iso_1 \\ iso_2 \end{bmatrix} \end{aligned} \quad (23)$$

where $k_{mtb} = M_{tb}/(L_t + L_b)$.

This result is important since it shows that the leakage inductance for each subsystem is different. Therefore, it is of interest to see how these inductances vary with the pitch. In general, coefficient k_{mtb} varies from 0.25 to 0.35 for open slots [3], depending on their shape only. For the slot shape of Fig. 1, and neglecting the flux through area G (which is not false for small-air-gap machines such as induction machines), k_{mtb} is

$$k_{mtb} = \frac{\left[d_3 + \frac{(d_1 - d_2)}{4} + \frac{d_4}{(1 - b/a)} \ln\left(\frac{a}{b}\right) + \frac{ad_5}{b} \right]}{\left[2d_3 + \frac{5(d_1 - d_2)}{6} + d_2 + \frac{2d_4}{(1 - b/a)} \ln\left(\frac{a}{b}\right) + 2\frac{ad_5}{b} \right]}. \quad (24)$$

As an example, k_{mtb} is plotted in Fig. 4, versus some slot dimensions, for given copper surface and slot width (the other dimensions have been fixed). It is observed that k_{mtb} is higher for semiclosed slots than for open slots. This is simply explained by a smaller slot top. In fact, if the width of the slot top is decreased, the magnetic field in this region is increased, which increases the mutual leakage inductance between top and bottom conductors.

Leakage inductance variations are plotted in Fig. 6 as a per unit of $(L_t + L_b)$, with $0.2 < k_{mtb} < 0.5$. An important observation is that a coil pitch of 5/6, so commonly used in three-phase motors, results in a very small value of L_{lsxy} , whereas the value of L_{lsdq} remains practically unchanged compared with its value for full pitch. Moreover, it is seen that the higher the value of k_{mtb} is, the larger the difference between $L_{lsxy}(r = 1)$ (highest value) and $L_{lsxy}(r = 5/6)$ (lowest value in the range $2/3 < r < 1$) is (see Fig. 5, ratio $L_{lsxy}(r = 1)/L_{lsxy}(r = 5/6)$). Note also in Fig. 5 that the ratio $L_{lsdq}(r = 1)/L_{lsdq}(r = 5/6)$ is practically unmodified by k_{mtb} . Consequently, full pitch is required to obtain a great $(x - y)$ leakage inductance, which will limit the amplitude of

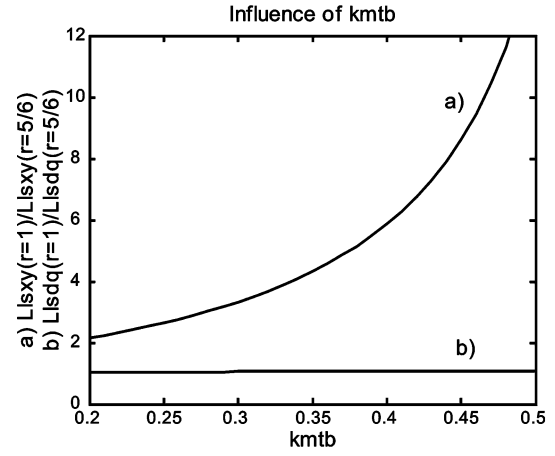


Fig. 5. Influence of k_{mtb} on ratios $L_{lsxy}(r = 1)/L_{lsxy}(r = 5/6)$ and $L_{lsdq}(r = 1)/L_{lsdq}(r = 5/6)$.

circulating harmonic currents as it will be shown in the next section. Special slot shape designs should also be investigated in order to increase k_{mtb} . But increasing k_{mtb} also results in increasing the $(d - q)$ leakage inductance and this will decrease the starting and pullout torque. However, since using full pitch increases the winding factor, the phase voltage should be increased to maintain the maximal air-gap flux density at a given value. This would compensate the deficiency in torque.

Finally, it is important to underscore that, even with full pitch, a dual-stator winding does not produce space harmonic below the 11th [8].

The basic rules proposed in this paper might be sufficient to avoid the use of an external filter [10]. If not, a built-in filter can be used [11]. Reference [11] has proposed a solution based on the same principle of mutual leakage coupling between the two stators, by adding magnetic rings in the end-winding zone.

2) *Complete Model for Simulation:* For the complete model, (13) must be completed with inductance matrices due to the main flux to obtain the total flux linked by the stator windings

$$[\Psi_s] = \{[L_{ls}] + [M_{lss}] + [L_{ms}] + [M_{mss}]\} [is] + [M_{sr}][ir]. \quad (25)$$

Similar equations apply for the three phase rotor windings

$$[\Psi_r] = {}^t[M_{sr}][is] + \{[L_{lr}] + [L_{mr}] + [M_{mrr}]\} [ir]. \quad (26)$$

Voltage equations are the following:

$$[vs] = [Rs][is] + \frac{d[\Psi_s]}{dt} \quad (27)$$

$$[vr] = [Rr][ir] + \frac{d[\Psi_r]}{dt} \quad (28)$$

$$[vs] = {}^t[vs_{a1} \ vs_{b1} \ vs_{c1} \ vs_{a2} \ vs_{b2} \ vs_{c2}] \quad (29)$$

$$[is] = {}^t[is_{a1} \ is_{b1} \ is_{c1} \ is_{a2} \ is_{b2} \ is_{c2}] \quad (30)$$

$$[\Psi_s] = {}^t[\Psi_{sa1} \ \Psi_{sb1} \ \Psi_{sc1} \ \Psi_{sa2} \ \Psi_{sb2} \ \Psi_{sc2}] \quad (31)$$

$$[vr] = {}^t[vra \ vrb \ vrc] \quad (32)$$

$$[ir] = {}^t[ira \ irb \ irc] \quad (33)$$

$$[\Psi_r] = {}^t[\Psi_{ra} \ \Psi_{rb} \ \Psi_{rc}] \quad (34)$$

and (35)–(41), as shown at the bottom of the next page.

The detail of the submatrices is given in (29)–(41). R_s and L_{ms} are the stator resistance and magnetizing inductance. R_r , L_{lr} , and L_{mr} are the rotor resistance, leakage inductance, and magnetizing inductance. N_s and N_r are the number of turns of the stator and rotor windings including winding factors.

After applying the transformation matrix $[Ts(\alpha)]^{-1}$ to stator variables and the Park's transformation to the rotor variables, the final model expressed in the stationary reference frame is given by the following equations:

$$\begin{bmatrix} vsd \\ vrd \\ vsq \\ vrq \end{bmatrix} = \begin{bmatrix} R_s & 0 & 0 & 0 \\ 0 & R_r & M\theta_1^\bullet & Lr\theta_1^\bullet \\ 0 & 0 & R_s & 0 \\ -M\theta_1^\bullet & -Lr\theta_1^\bullet & 0 & R_r \end{bmatrix} \begin{bmatrix} isd \\ ird \\ isq \\ irq \end{bmatrix} + \begin{bmatrix} L_s & M & 0 & 0 \\ M & L_r & 0 & 0 \\ 0 & 0 & L_s & M \\ 0 & 0 & M & L_r \end{bmatrix} \frac{d}{dt} \begin{bmatrix} isd \\ ird \\ isq \\ irq \end{bmatrix} \quad (42)$$

$$\begin{bmatrix} vsx \\ vsy \end{bmatrix} = \begin{bmatrix} R_s & 0 \\ 0 & R_s \end{bmatrix} \begin{bmatrix} isx \\ isy \end{bmatrix} + \begin{bmatrix} L_{lsxy} & 0 \\ 0 & L_{lsxy} \end{bmatrix} \frac{d}{dt} \begin{bmatrix} isx \\ isy \end{bmatrix} \quad (43)$$

$$\begin{bmatrix} vso_1 \\ vso_2 \\ vro \end{bmatrix} = \begin{bmatrix} R_s & 0 & 0 \\ 0 & R_s & 0 \\ 0 & 0 & R_r \end{bmatrix} \begin{bmatrix} iso_1 \\ iso_2 \\ iro \end{bmatrix} + \begin{bmatrix} L_{lso} & 0 & 0 \\ 0 & L_{lso} & 0 \\ 0 & 0 & L_{lr} \end{bmatrix} \frac{d}{dt} \begin{bmatrix} iso_1 \\ iso_2 \\ iro \end{bmatrix} \quad (44)$$

$$Te = pM(isq ird - isd irq) \quad (45)$$

$$\frac{d\theta_1}{dt} = \Omega_M \quad (46)$$

$$\frac{d\Omega_M}{dt} = \frac{1}{J}(Te - Tc) \quad (47)$$

where $L_s = L_{lsdq} + 3L_{ms}$, $M = (3M_{sr}/\sqrt{2})$, and $L_r = L_{lr} + (3/2)L_{mr}$.

θ_1 is the mechanical position of the rotor with respect to stator phase a_1 , Ω_M is the mechanical speed, Te and Tc are the electromagnetic and load torque, and J is the rotor inertia.

Equation (45) shows that $(x-y)$ currents do not contribute to torque production, and (43) relates $(x-y)$ currents only to stator resistance and leakage inductance. It is clear from the above equations that, in order to avoid extra losses in the machine, the $(x-y)$ leakage inductance should be as high as possible. As shown in Fig. 6, this can be achieved by using full pitch.

$$[L_{ms}] + [M_{mss}] = L_{ms} \begin{bmatrix} 1 & \cos(\frac{2\pi}{3}) & \cos(\frac{4\pi}{3}) & \cos(\alpha) & \cos(\alpha + \frac{2\pi}{3}) & \cos(\alpha + \frac{4\pi}{3}) \\ \cos(\frac{4\pi}{3}) & 1 & \cos(\frac{2\pi}{3}) & \cos(\alpha - \frac{2\pi}{3}) & \cos(\alpha) & \cos(\alpha + \frac{2\pi}{3}) \\ \cos(\frac{2\pi}{3}) & \cos(\frac{4\pi}{3}) & 1 & \cos(\alpha - \frac{4\pi}{3}) & \cos(\alpha - \frac{2\pi}{3}) & \cos(\alpha) \\ \cos(\alpha) & \cos(\alpha - \frac{2\pi}{3}) & \cos(\alpha - \frac{4\pi}{3}) & 1 & \cos(\frac{2\pi}{3}) & \cos(\frac{4\pi}{3}) \\ \cos(\alpha + \frac{2\pi}{3}) & \cos(\alpha) & \cos(\alpha - \frac{2\pi}{3}) & \cos(\frac{4\pi}{3}) & 1 & \cos(\frac{2\pi}{3}) \\ \cos(\alpha + \frac{4\pi}{3}) & \cos(\alpha + \frac{2\pi}{3}) & \cos(\alpha) & \cos(\frac{2\pi}{3}) & \cos(\frac{4\pi}{3}) & 1 \end{bmatrix} \quad (35)$$

$$[R_s] = R_s \begin{bmatrix} 1 & 0 & 0 & 0 & 0 & 0 \\ 0 & 1 & 0 & 0 & 0 & 0 \\ 0 & 0 & 1 & 0 & 0 & 0 \\ 0 & 0 & 0 & 1 & 0 & 0 \\ 0 & 0 & 0 & 0 & 1 & 0 \\ 0 & 0 & 0 & 0 & 0 & 1 \end{bmatrix} \quad (36)$$

$${}^t[M_{sr}(\theta_1)] = M_{sr} \times \begin{bmatrix} \cos(\theta_1) & \cos(\theta_1 - \frac{2\pi}{3}) & \cos(\theta_1 - \frac{4\pi}{3}) & \cos(\theta_1 - \alpha) & \cos(\theta_1 - \alpha - \frac{2\pi}{3}) & \cos(\theta_1 - \alpha - \frac{4\pi}{3}) \\ \cos(\theta_1 + \frac{2\pi}{3}) & \cos(\theta_1) & \cos(\theta_1 - \frac{2\pi}{3}) & \cos(\theta_1 - \alpha + \frac{2\pi}{3}) & \cos(\theta_1 - \alpha) & \cos(\theta_1 - \alpha - \frac{2\pi}{3}) \\ \cos(\theta_1 + \frac{4\pi}{3}) & \cos(\theta_1 + \frac{2\pi}{3}) & \cos(\theta_1) & \cos(\theta_1 - \alpha + \frac{4\pi}{3}) & \cos(\theta_1 - \alpha + \frac{2\pi}{3}) & \cos(\theta_1 - \alpha) \end{bmatrix} \quad (37)$$

$$L_{lr} = \begin{bmatrix} 1 & 0 & 0 \\ 0 & 1 & 0 \\ 0 & 0 & 1 \end{bmatrix} \quad (38)$$

$$[L_{mr}] + [M_{mrr}] = L_{mr} \begin{bmatrix} 1 & \cos(\frac{2\pi}{3}) & \cos(\frac{4\pi}{3}) \\ \cos(\frac{4\pi}{3}) & 1 & \cos(\frac{2\pi}{3}) \\ \cos(\frac{2\pi}{3}) & \cos(\frac{4\pi}{3}) & 1 \end{bmatrix} \quad (39)$$

$$[R_r] = R_r \begin{bmatrix} 1 & 0 & 0 \\ 0 & 1 & 0 \\ 0 & 0 & 1 \end{bmatrix} \quad (40)$$

$$M_{sr} = \frac{N_r}{N_s} L_{ms} \quad (41)$$

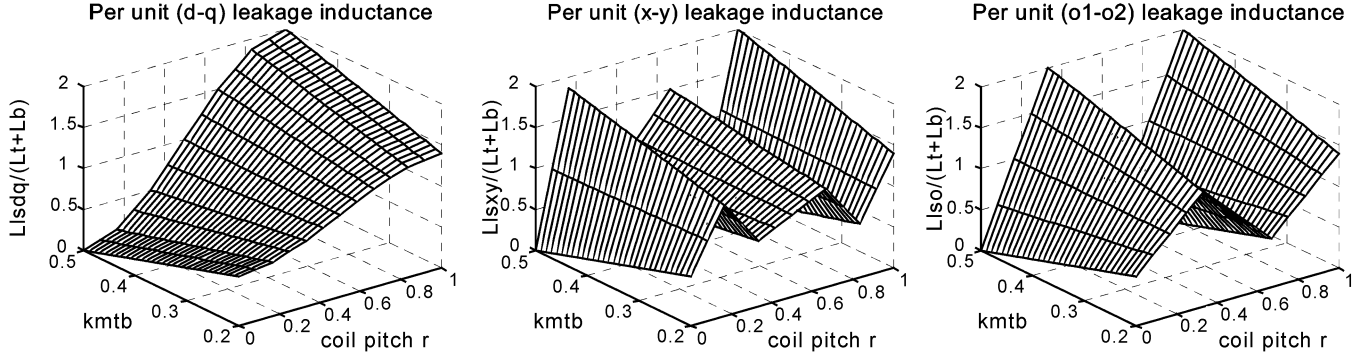


Fig. 6. From left to right: per-unit leakage inductances versus coil pitch r and coefficient k_{mtb} , for $(d - q)$, $(x - y)$, and $(o_1 - o_2)$ equivalent circuits.

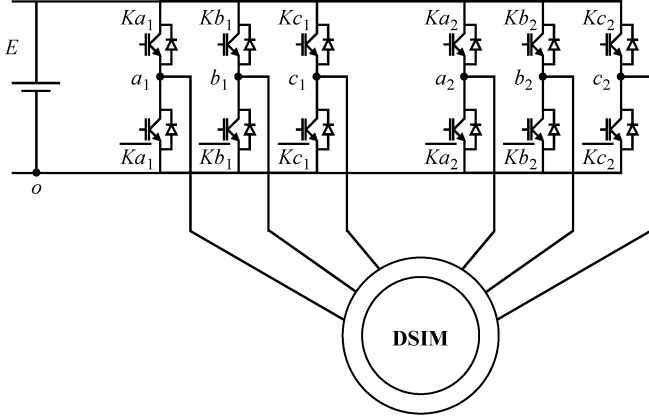


Fig. 7. Six-phase VSI-fed DSIM.

In addition to maximizing this $(x - y)$ leakage inductance, the applied voltages should also contain minimum amplitude $(x - y)$ components. An appropriate space-vector pulsewidth-modulation PWM strategy can achieve this [4], [5].

V. SIMULATION RESULTS

In general, the leakage flux can be divided into slot, end-winding, belt, and zig-zag components, and each of them contributes to the self- and mutual leakage inductance [2], [3]. With reasonable approximation, the end-winding leakage components can be assumed to vary as the slot leakage. For simplicity, it is assumed here that the remaining components only contribute to the self-leakage. Therefore, in the model for the simulation, the following inductances have been used:

- $Lls = (L_t + L_b) + \text{other "self-leakage" components}$;
- $Mls = M_{tb} + \text{other "mutual leakage" components}$.

With a ratio $Mls/Lls = 0.35$, it is obtained that: $Llsxy(r = 1) = 1.7Lls$, $Llsxy(r = 5/6) = 0.393Lls$, $Llsdq(r = 1) = 1.7Lls$, and $Llsdq(r = 5/6) = 1.606Lls$.

The drive system is a dual three-leg VSI-fed DSIM as shown in Fig. 7. A sine-triangle PWM operation has been simulated with the parameters of a 1.4-MW machine [14], for the 5/6-pitch and the full-pitch cases. For these two configurations, the change in leakage inductances $Llsdq$ and $Llsxy$, as well as the change in the winding factor (change in inductances Lms and Msr), has been taken into account. Simulation results are

shown in Fig. 8 and Table II. As expected, it is observed that phase current peaks due to $(x - y)$ components are greatly reduced by the simple use of a full-pitch winding rather than a 5/6-pitch one. This reduction is more significant when high order harmonics, depending on the switching frequency, are considered. Due to the small increase in $Llsdq$ and in the winding factor, it is also noted in Table II that the fundamental component of the phase current is slightly inferior in the full-pitch case.

In order to illustrate the effect that using full pitch has on torque, a steady-state analysis, with balanced sinusoidal voltage excitation, has been made using the usual per-phase equivalent circuit [3]. Note that with this kind of excitation, the model of the DSIM reduces to $(d - q)$ equations. The torque-slip curves obtained for the same machine with a 5/6-pitch and a full-pitch winding are plotted in Fig. 9. Case 0 corresponds to $r = 5/6$, while other cases correspond to $r = 1$. In cases 0, 1, and 2, the phase voltage is kept the same whereas in case 3 it is increased by the same percentage as the winding factor. In case 1, where only the increase in $Llsdq$ is considered, the torque is slightly reduced compared with the one obtained for case 0. Case 2 and case 3 are more realistic since both increases in $Llsdq$ and in winding factor are considered. Case 2 shows that the torque is still reduced. However, as mentioned in Section IV-B-1), it is observed in case 3 that adjusting the phase voltage allows compensating for this deficiency in torque.

To summarize, the use of a full-pitch winding rather than a 5/6-pitch one has the following effects.

- 1) Inductance $Llsxy$ is greatly increased, which leads to minimize circulating harmonic currents and which has no effect on torque and on the fundamental current.
- 2) Inductance $Llsdq$ is only slightly increased, which leads to a small reduction of the torque and of the fundamental current.
- 3) The winding factor is increased, making possible an increase in the phase voltage so that the deficiency in torque is compensated.

Moreover, as shown in the previous section, an increase in k_{mtb} results in an increase of both $Llsxy$ and $Llsdq$ for full pitch. Therefore, optimization of slot shapes should be considered in order to find a suitable value of k_{mtb} .

Beyond this analysis, it is clear that the study of all these parameters has to be included in the global design of the full-pitch-winding machine.

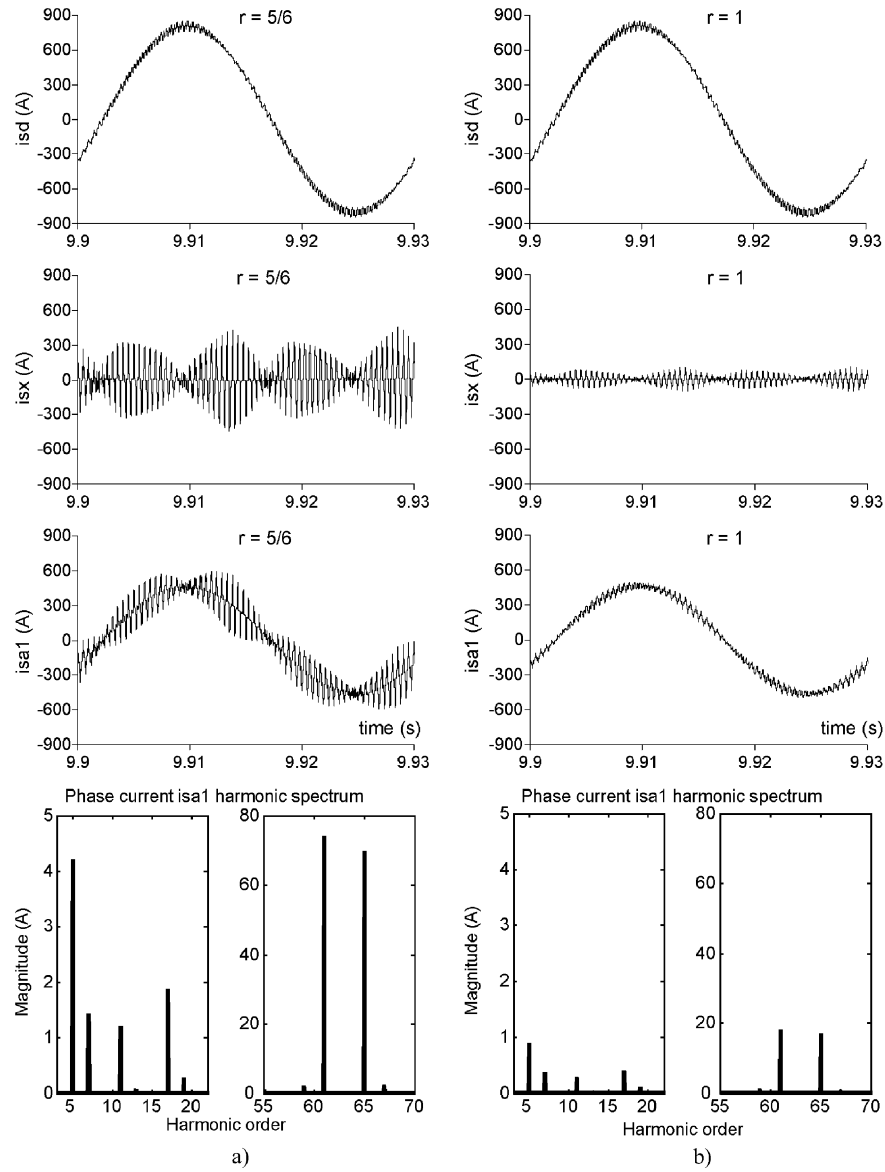


Fig. 8. Simulation results of sine-triangle PWM operation with $MIs/LIs = 0.35$. From top to bottom: d -axis current, x -axis current, phase current, phase current harmonic spectrum. (a) $r = 5/6$. (b) $r = 1$.

TABLE II
RELATIVE PERCENTAGE OF PHASE CURRENT HARMONICS (SEE FIG. 8) FOR
FULL PITCH ($I_h(r = 1)/I_h(r = 5/6)$)

1 st	5 th	7 th	59 th	61 st	65 th	67 th
97.48 %	21.38 %	25.63 %	24.02 %	24.38 %	24.47 %	25.46 %

VI. EXPERIMENTAL RESULTS

In order to validate the model including mutual leakage coupling, a prototype of a squirrel-cage induction motor has been rewound so that all the coils are accessible (a photograph is in the Appendix). Some tests, consisting of the identification of the leakage inductance of $(d-q)(x-y)(o_1-o_2)$ circuits, have been performed for different coil pitches.

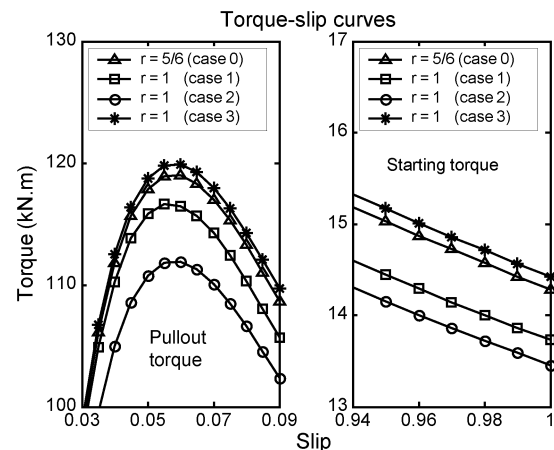


Fig. 9. Torque-slip curves. Case 1: neglecting the increase in winding factor; case 2: including the increase in winding factor; and case 3: case 2 with a phase voltage increased by the same percentage as the winding factor.

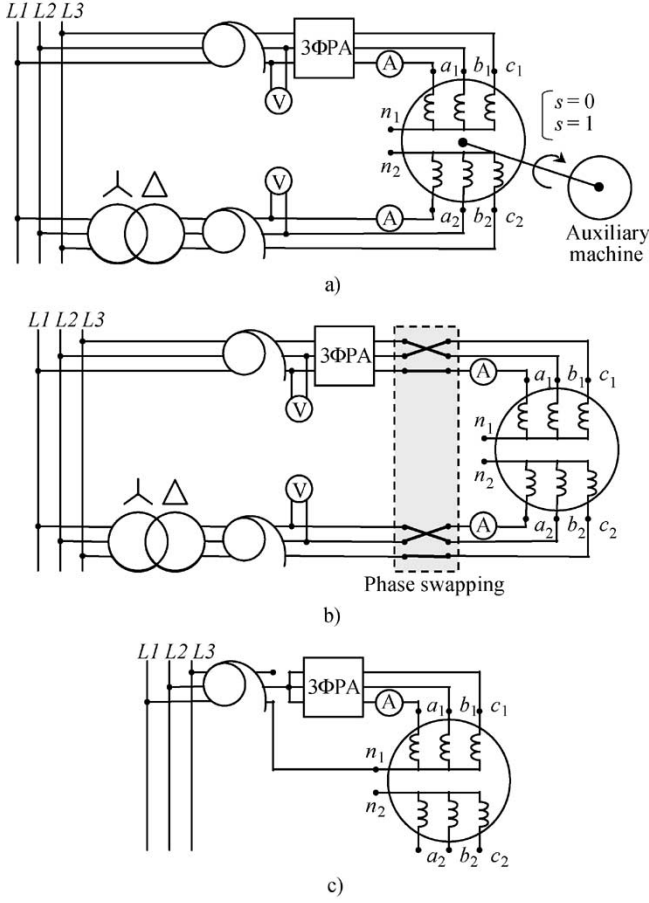


Fig. 10. Wiring schemes for the identification of leakage inductances. (a) $(d-q)$ tests. (b) $(x-y)$ test. (c) $(o_1 - o_2)$ test.

A. “ $(d-q)$ Tests”

The $(d-q)$ tests consist in exciting the DSIM by a balanced set of $(d-q)$ sequence voltages. The $(d-q)$ sequence is given by the arguments of the cosine or sine terms of the first or second row in transformation matrix $[Ts(\alpha)]^{-1}$. Hence, only the $(d-q)$ subsystem is excited so that it is possible to identify only $(d-q)$ parameters. These tests are sketched in Fig. 10(a). The star-delta transformer has been used to obtain a time shift of 30° in the voltages. The first test has been made at zero slip ($s = 0$) in order to identify the stator main inductance

$$Ls = \frac{6E^2}{\omega s Q_{6\phi}} \quad (48)$$

where ωs denotes the synchronism speed and $Q_{6\phi}$ the reactive power measured for the whole six phases. E is the electromotive force, calculated from voltage, current, and dc stator resistance measurements.

Since the rotor is a standard squirrel cage, $(d-q)$ leakage inductance $Llsdq$ cannot be extracted from Ls . Therefore, a locked-rotor test ($s = 1$) has been made to identify leakage factor σ . Hence, parameter σLs is used as a figure of merit, instead of the nonmeasurable $Llsdq$

$$\sigma Ls \approx Llsdq + 2 \left(\frac{Ns}{Nr} \right)^2 Llr. \quad (49)$$

σLs includes the referred-to-stator rotor leakage inductance. Therefore, the difference with $Llsdq$ alone can be expected to be maximal at $r = 1$ (where Ns is maximal), and nil at $r = 0$ (where Ns is zero).

B. “ $(x-y)$ Test”

The $(x-y)$ test consists in exciting the DSIM by a balanced set of $(x-y)$ sequence voltages. The $(x-y)$ sequence is given by the arguments of the cosine or sine terms of the third or fourth row in transformation matrix $[Ts(\alpha)]^{-1}$. This test is sketched in Fig. 10(b). Hence, only the $(x-y)$ subsystem is excited so that it is possible to isolate the $(x-y)$ leakage inductance

$$Llsxy = \frac{6E^2}{\omega s Q_{6\phi}}. \quad (50)$$

C. “ $(o_1 - o_2)$ Test”

This test has been made with a zero-sequence voltage excitation. It is sketched in Fig. 10(c) and has been performed for each stator (see two last rows in $[Ts(\alpha)]^{-1}$). Hence, the $(o_1 - o_2)$ leakage inductance can be obtained

$$Llso = \frac{3E^2}{\omega s Q_{3\phi}}. \quad (51)$$

The reactive power measurement has been made with a three-phase power analyzer (3ϕ PA). In order to guarantee balanced excitations for the $(d-q)$ and $(x-y)$ tests, the voltages have been increased and decreased step by step, and the measures have been taken at different voltage levels when the two amperemeters show equal values. This guarantee balanced sets of voltages of the corresponding sequence. In this case, the total power is simply two times the one measured by the 3ϕ PA (assuming identical parameters for the two stators). A considerable amount of data have been collected and the inductances have been calculated from (48), (49), (50), and (51), by linear interpolation of curves $Q = f(E^2)$ in the nonsaturation range, for the seven possible coil pitch connections.

The results are given in Fig. 11(a)–(c). It is observed that the variations of $(d-q)$, $(x-y)$ and $(o_1 - o_2)$ leakage inductances, according to the coil pitch, are in total agreement with those expected by theory. However, as shown in Fig. 6, the three leakage inductances should normally have the same value for $r = 1/2$. In particular, for that value of the coil pitch, one should identify self-leakage inductance Lls . It can be seen in Fig. 11 that there exists a difference between the experimental values of $Llsxy(r = 1/2)$ and $Llso(r = 1/2)$. This difference can be explained by the fact that the mutual leakage coupling due to belt and zig-zag components has been neglected. Therefore, for a purpose of comparison, two theoretical curves are also plotted, one assuming that $Lls = Llsxy(r = 1/2)$ and the other assuming that $Lls = Llso(r = 1/2)$. These curves are plotted with coefficient k_{mtb} equal to 0.4348, taken from Fig. 5 with experimental ratio $Llsxy(r = 1)/Llsxy(r = 5/6)$ equal to 7.5753. One can see that with the corresponding value of Lls , theoretical and experimental curves are superimposed. It is clear from these observations that machine leakage inductances are proportional to those given by Fig. 6.

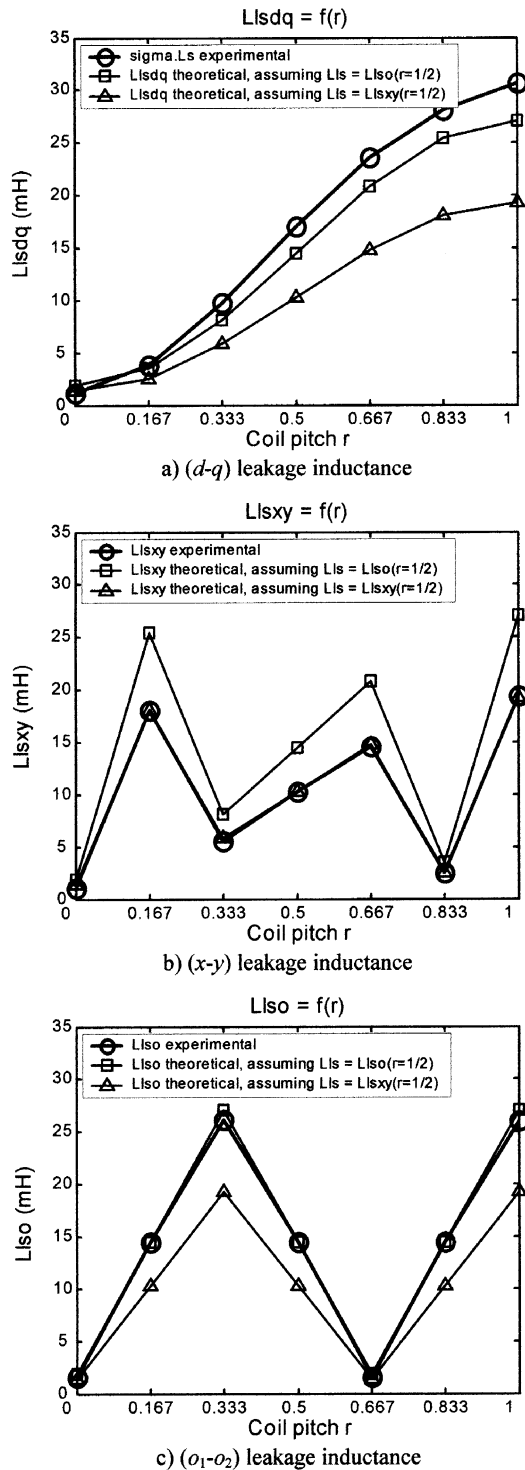


Fig. 11. Comparison of theoretical and experimental values of leakage inductances.

Note that coefficient k_{mtb} is high. This is probably due to the slot shape used in this small machine. Therefore, during a PWM operation, the improvement using full pitch would be still better than the one presented in Fig. 8. PWM tests are in progress, and they will be reported in the near future.

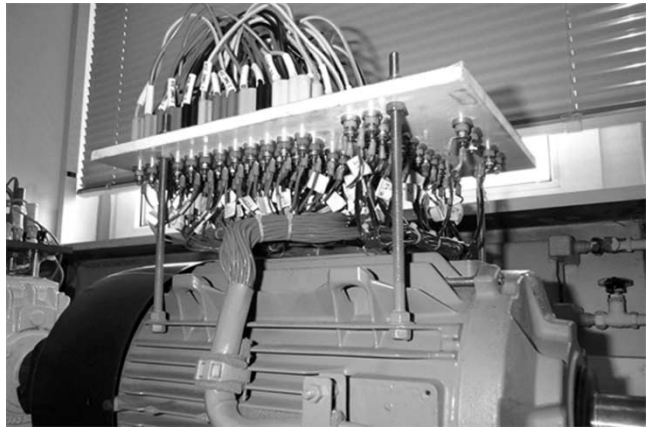


Fig. 12. Machine prototype used for the tests.

VII. CONCLUSION

A new reference frame model of dual-stator winding induction machines, including mutual leakage coupling, has been presented in this paper. It has been shown that the coil pitch has a great influence on the impedance value associated with circulating harmonic currents. It has been also shown that full pitch is required, and that special slot shape designs should be investigated, to limit the magnitude of these circulating currents. Experimental results on a prototype of a DSIM have been presented and they show a very good correlation with theoretical curves. Therefore, particular attention must be paid to the design of dual-stator winding ac machines for safe operation with a VSI.

It must be noted that this paper is the first part of a study that leads to the design of a new safety dual-stator winding, eliminating circulating harmonic currents, and minimizing air-gap flux space harmonics.

APPENDIX

The machine on which the tests were run is a rewound eight-pole 15-kW squirrel-cage induction motor (see Fig. 12). It has the leads from each of its 48 stator coils brought out to a terminal board. The 96 terminals can, therefore, be connected in many different ways for different pole numbers, phase numbers and coil pitches. In fact, each coil has a full pitch, but thanks to the terminal board, it is possible to obtain the same distribution of conductors as coil pitches varying from 1 to 0, with an increment of $1/6$.

ACKNOWLEDGMENT

The authors wish to thank Dr. T. Lubin of the G.R.E.E.N. laboratory, Université H. Poincaré, Nancy, France, for his valuable suggestions and helpful discussions, and Dr. P. Manfé of Leroy-Somer Company, Angoulême, France, for his technical support in the development of the experimental bench.

REFERENCES

- [1] P. L. Alger, E. H. Freiburghouse, and D. D. Chase, "Double windings for turbine alternators," *AIEE Trans.*, vol. 49, pp. 226–244, Jan. 1930.
- [2] P. L. Alger, *Induction Machines*, 2nd ed. New York: Gordon and Breach, 1970.

- [3] T. A. Lipo, "A d-q model for six phase induction machines," in *Proc. Int. Conf. Electric Machines*, Athens, Greece, 1980, pp. 860–867.
- [4] Y. Zhao and T. A. Lipo, "Space vector PWM control of dual three phase induction machine using vector space decomposition," *IEEE Trans. Ind. Applicat.*, vol. 31, pp. 1100–1109, Sept./Oct. 1995.
- [5] D. Hadiouche, H. Razik, and A. Rezzoug, "Study and simulation of space vector PWM control of double-star induction motors," in *Proc. IEEE-CIEP 2000*, Acapulco, Mexico, Oct. 15–19, 2000, pp. 42–47.
- [6] M. A. Abbas, R. Christen, and T. M. Jahns, "Six-phase voltage source inverter driven induction motor," *IEEE Trans. Ind. Applicat.*, vol. IA-20, pp. 1251–1259, Sept./Oct. 1984.
- [7] K. Gopakumar, V. T. Ranganathan, and S. R. Bhat, "Split phase induction motor operation from PWM voltage source inverter," *IEEE Trans. Ind. Applicat.*, vol. 29, pp. 927–932, Sept./Oct. 1993.
- [8] E. A. Klingshirn, "High phase order induction motors Part I—description and theoretical considerations," *IEEE Trans. Power App. Syst.*, vol. PAS-102, pp. 47–53, Jan. 1983.
- [9] —, "High phase order induction motors Part II—experimental results," *IEEE Trans. Power App. Syst.*, vol. PAS-102, pp. 54–59, Jan. 1983.
- [10] K. Oguchi, A. Kawaguchi, T. Kubota, and N. Hoshi, "A novel six-phase inverter system with 60-step output voltages for high-power motor drives," *IEEE Trans. Ind. Applicat.*, vol. 35, pp. 1141–1149, Sept./Oct. 1999.
- [11] L. Xu and L. Ye, "Analysis of a novel winding structure minimizing harmonic current and torque ripple for dual six-step converter-fed high power AC machines," *IEEE Trans. Ind. Applicat.*, vol. 31, pp. 84–90, Jan./Feb. 1995.
- [12] R. H. Nelson and P. C. Krause, "Induction machine analysis for arbitrary displacement between multiple winding sets," *IEEE Trans. Power App. Syst.*, vol. PAS-93, pp. 841–848, May/June 1974.
- [13] E. Andersen and K. Bieniek, "6-phase induction motors for current source inverter drives," in *Conf. Rec. IEEE-IAS Annu. Meeting*, 1981, pp. 607–618.
- [14] A. Monti, A. P. Morando, L. Resta, and M. Riva, "Comparing two level GTO-inverter feeding a double star asynchronous motor with a three level GTO-inverter feeding a single star asynchronous motor," in *Proc. EPE'95*, Seville, Spain, Sept. 19–21, 1995, pp. 2.419–2.425.
- [15] J. Huang, "Application of the transformation for p-pole n-phase system to the analysis of the 2×3 phase induction motors," in *Proc. IECM'94*, vol. 2, Paris, France, Sept. 5–8, 1994, pp. 591–595.
- [16] E. E. Ward and H. Härer, "Preliminary investigation of an inverter-fed 5-phase induction motor," *Proc. Inst. Elect. Eng.*, vol. 116, no. 6, pp. 980–984, June 1969.
- [17] J. R. Stewart and D. D. Wilson, "High phase order transmission—a feasibility analysis, part I—steady state consideration," *IEEE Trans. Power App. Syst.*, vol. PAS-97, pp. 2300–2307, Nov./Dec. 1978.
- [18] K. N. Pavithran, R. Parimelalagan, and M. R. Krishnamurthy, "Studies on inverter-fed five phase induction motor drive," *IEEE Trans. Power Electron.*, vol. 3, pp. 224–235, Apr. 1988.
- [19] D. Hadiouche, H. Razik, and A. Rezzoug, "Design of novel winding configurations for VSI fed dual-stator induction machines," in *Proc. ELECTRIMACS 2002*, Montreal, QC, Canada, Aug. 18–21, 2002, CD-ROM.



Djafar Hadiouche received the Ph.D. degree in electrical engineering from the University Henri Poincaré, Nancy, France, in 2001.

From 2001 to 2002, he was Assistant Lecturer at the University Henri Poincaré and conducted research in the laboratory of the "Groupe de Recherche en Electrotechnique et Electronique de Nancy." He is currently a Motion Specialist Engineer with GE Fanuc Automation Europe, Echternach, Luxembourg. His main research interests concern multiphase ac machines and their modeling, identification, PWM techniques, and vector control.

Dr. Hadiouche received the Best Prize Paper Award from the Electric Machine Committee at the 2001 IEEE Industry Application Society Annual Meeting.



Hubert Razik (M'98–SM'03) was born in Pompey, France, in 1962. He graduated from the Ecole Normale Supérieure, Cachan, France, in 1987, received the Ph.D. degree in electrical engineering from the Polytechnic Institute of Lorraine, Nancy, France, in 1991, and received the "Habilitation à Diriger des Recherches" degree from the University Henri Poincaré, Nancy, France, 2000.

In 1993, he joined the "Groupe de Recherche en Electrotechnique et Electronique de Nancy," Nancy, France, as an Assistant Professor. He is currently an

Associate Professor of Electrical Engineering at the University Henri Poincaré. He has authored or coauthored more than 50 scientific conference and journal papers. His fields of research concern the modeling, control, and diagnostics of multiphase induction motors.



Abderrezak Rezzoug (M'79) is a Professor of Electrical Engineering at the University Henri Poincaré, Nancy, France. As the head of the "Groupe de Recherche en Electrotechnique et Electronique de Nancy," his main subjects of research concern electrical machines, their identification, diagnostics, and control, and superconducting applications.